SPATIOTEMPORAL DISTRIBUTION AND DRIVING MECHANISMS OF NET PRIMARY PRODUCTIVITY IN THE SHIGATSE REGION, CHINA, BASED ON RANDOM FOREST AND SHAP

LIU, C. Y.[1] – YU, W.[2*]

[1]*College of Forestry and Grassland Science, Xizang Agricultural and Animal Husbandry University, 860000 Xizang, Nyingchi, China*
(phone: +86-198-5350-2327)

[2]*College of Resources and Environment, Soil and Water Conservation Talent Innovation Base, XiZang Agricultural and Animal Husbandry University, 860000 Xizang, Nyingchi, China*

**Corresponding author*
e-mail: yuwu4270@126.com; phone: +86-156-8942-4118

(Received 10th Nov 2025; accepted 18th Feb 2026)

Abstract. This study assesses the spatiotemporal dynamics of Net Primary Productivity (NPP) and its driving factors in the climate-sensitive Shigatse region, China. We reconstructed a 30-m resolution NDVI dataset using the Enhanced Spatial and Temporal Adaptive Reflectance Fusion Model to drive the Carnegie-Ames-Stanford Approach model for growing seasons (July–September) from 2000 to 2023. Random Forest and SHAP analyses were integrated to decouple driving forces. Results indicate an increasing NPP trend (0.75 g C m^{-2} $year^{-1}$) with a distinct "high-east, low-west" spatial pattern. The conversion of barren land to grassland was the primary driver of this increase. Elevation acted as the dominant limiting factor, significantly inhibiting NPP above 5000 m. Optimal growth conditions were identified as precipitation exceeding 100 mm, mean temperature of 6–10°C, and solar radiation exceeding 1400 W/m^2 (during the growing season). In conclusion, NPP improvement is primarily attributed to land cover transitions from barren land to grassland, while hydrothermal conditions, governed by vertical differentiation in elevation, remain the core forces shaping spatiotemporal patterns.
Keywords: *carbon sequestration, ESTARFM, climate sensitivity, ecological restoration, Tibetan Plateau*

Introduction

Net Primary Productivity (NPP) serves as a core indicator of ecosystem health and carbon sequestration potential by quantifying the net organic matter fixed by vegetation through photosynthesis (Potter et al., 1993; Field et al., 1998). As a complex ecological process, the spatiotemporal dynamics of NPP are governed by the interplay of climatic factors (e.g., temperature, precipitation, and solar radiation), land use/land cover change (LULCC), and anthropogenic activities (Running et al., 2004; Piao et al., 2020). These factors significantly influence plant photosynthesis and respiration, ultimately determining regional NPP patterns (Mayer et al., 2021). Therefore, accurately assessing spatiotemporal variations in NPP and quantitatively decoupling its driving mechanisms are fundamental for understanding ecosystem responses to climate change, evaluating carbon budgets, and formulating sustainable development strategies (Chen et al., 2019; Zhang et al., 2023).

Shigatse, located on the southwestern border of China and in the southern region of the Tibetan Plateau, is home to Mount Everest and the source of the Yarlung Zangbo River (Cai et al., 2017). The Gangdise and Himalayan Mountain ranges within this region form a crucial ecological barrier, making the stability of its ecosystem decisive for the sustainable development of the entire plateau (Basang et al., 2022; Nayak et al., 2023). Against the backdrop of escalating global climate change, the high-altitude cold

http://www.aloki.hu ● ISSN 1589 1623 (Print) ● ISSN 1785 0037 (Online)
DOI: http://dx.doi.org/10.15666/aeer/2402_33753391

ecosystem of Shigatse is particularly sensitive to climatic disturbances (Scholze et al., 2006). As a central hub connecting the atmosphere, hydrosphere, and biosphere, even minor changes in Shigatse's terrestrial ecosystem could exert a critical regulatory effect on the carbon cycle of the region and the wider Tibetan Plateau, rendering it an ideal area for studying ecosystem responses to climate change (Naeem et al., 2020).

In recent years, remote sensing has become the primary method for large-scale ecological monitoring (Wang et al., 2024). Among various models, the improved Carnegie-Ames-Stanford Approach (CASA) model has demonstrated strong stability in NPP inversion across various scales and is widely used globally (Potter et al., 1993; Zhu et al., 2007). While data from the Moderate Resolution Imaging Spectroradiometer (MODIS) provide the high temporal resolution required for CASA, their coarse spatial resolution limits their application in heterogeneous landscapes like Shigatse. To address this trade-off, spatiotemporal fusion algorithms, such as the Enhanced Spatial and Temporal Adaptive Reflectance Fusion Model (ESTARFM), have been proposed to fuse MODIS and Landsat data (Zhu et al., 2010). This approach generates synthetic data with both high spatial and temporal resolution and has been successfully validated in complex terrains (Emelyanova et al., 2013; Wu et al., 2022). Furthermore, advanced machine learning techniques, particularly Random Forest (RF) combined with SHAP (SHapley Additive exPlanations), provide robust means to interpret complex, non-linear ecological relationships (Breiman, 2001).

This study focuses on the Shigatse region, China, aiming to achieve the following three objectives: (1) To systematically reveal the spatiotemporal evolution patterns of NPP in the Shigatse region from 2000 to 2023; (2) to analyze the land cover type transitions and their specific impacts on NPP dynamics; and (3) to employ a combination of Random Forest and SHAP analysis to quantitatively decouple the interactive effects of key factors on NPP changes. These findings will provide a scientific basis for the ecological protection and adaptive management of high-altitude ecosystems.

Materials and methods

Study area

This study focuses on the Shigatse region (*Fig. 1*), located between 27°13′–31°49′ N and 82°1′–90°20′ E in the southwestern part of the Tibetan Plateau, China, with a total area of approximately 17.92×10^4 km². The region's topography is extremely complex and rugged, with an average elevation exceeding 4000 m. The Himalayan and Gangdise-Nyenchen Tanglha mountain ranges traverse the area, forming significant ecological and climatic barriers (Jiang, 2017; Wu et al., 2016; Xu et al., 2024). The Yarlung Zangbo River and its main tributary, the Nyangchu River, run through it, creating relatively flat and open river valley plains, which are the most densely populated and agriculturally concentrated areas in the region (Li and Xiao, 2024). The Shigatse region has a typical plateau temperate semi-arid monsoon climate, with significant horizontal and vertical zonation of hydrothermal conditions. Annual precipitation decreases sharply from approximately 430 mm in the southeast to less than 200 mm in the northwest (Zhou et al., 2011), while the mean annual temperature, primarily controlled by elevation, decreases from 6.5°C in the eastern valleys to below 0°C in the high-altitude western regions (Dunzhu et al., 2000). The dominant land cover types are grassland, shrubland, and forest (Gao et al., 2020). During the study period (2000–2023, July–September), the region's mean annual precipitation was approximately 136.75 mm, and the mean annual

http://www.aloki.hu ● ISSN 1589 1623 (Print) ● ISSN 1785 0037 (Online)
DOI: http://dx.doi.org/10.15666/aeer/2402_33753391

temperature fluctuated around 6.43°C. These climatic conditions serve as the fundamental environmental background driving the variations in NPP. Notably, approximately 9% of the total study area consists of non-vegetated surfaces, such as permanent snow, glaciers, and water bodies. Consequently, these areas were excluded from the NPP simulation and analysis in this study.

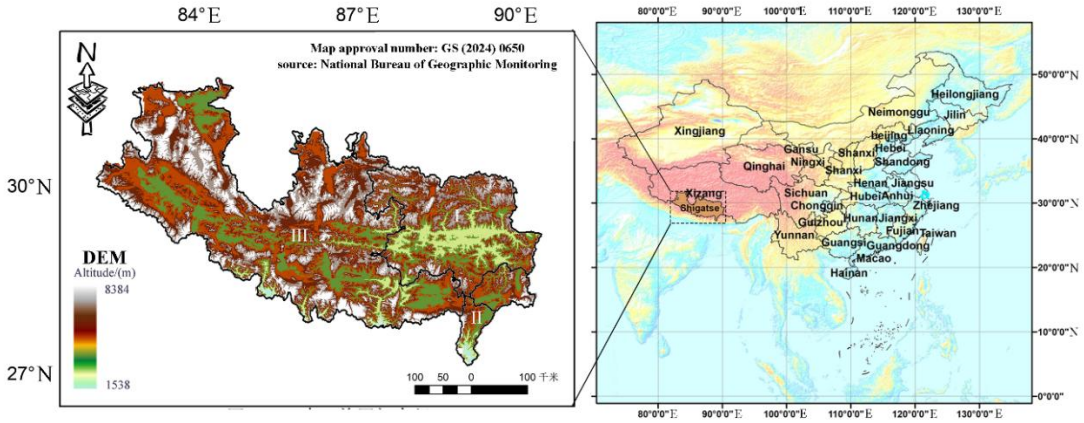

Figure 1. *Location and elevation map of the study area, Shigatse*

Data sources and pre-processing

Based on previous research on the Tibetan Plateau, the influencing factors of NPP can be broadly divided into three categories (*Table 1*): topography, climate, and human activities (Peng et al., 2021; Li et al., 2025). This study selected DEM, mean monthly temperature, total monthly precipitation, total monthly solar radiation, and human footprint data as the primary influencing factors. All data were pre-processed and standardized on the Google Earth Engine (GEE) platform and in local ENVI 6.3/ArcGIS Pro environments. To minimize the impact of phenological variations, satellite images were specifically selected from the peak growing season (July to September) for each year. To match the monthly computational step of the CASA model, daily precipitation and solar radiation data were aggregated to monthly totals, and daily mean temperature data were averaged to monthly values.

Research methods

ESTARFM-based NDVI time-series reconstruction

The ESTARFM model integrates the spatial advantages of 30-m Landsat data with the high temporal resolution of MODIS to monitor dynamic changes (Zhu et al., 2010). The method estimates a Landsat image at a prediction date based on two pairs of reference Landsat–MODIS images and one MODIS image at the prediction time. The fusion is calculated as *Equation 1*:

$$R_{fuse}(x,y,t) = W_{space}(x,y) \cdot W_{time}(t) \cdot R_l(x,y,t) \quad \text{(Eq.1)}$$

where $R_l(x,y,t)$ is the pixel value of the coarse image, $W_{space}(x,y)$ and $W_{time}(t)$ serve as the spatial and temporal adaptive weighting coefficients, respectively, and $R_{fuse}(x,y,t)$ is the final fused image.

http://www.aloki.hu ● ISSN 1589 1623 (Print) ● ISSN 1785 0037 (Online)
DOI: http://dx.doi.org/10.15666/aeer/2402_33753391

Table 1. *Data sources and their resolutions*

Data type	Dataset/product name	Source/platform	Spatiotemporal resolution	Time range
Meteorological	China 1-km monthly mean temperature	National Tibetan Plateau Data Center	1000 m, monthly	2000-2023 (accessed on 12 December 2024)
	China 1-km monthly precipitation	National Tibetan Plateau Data Center	1000 m, monthly	2000-2023 (accessed on 12 December 2024)
	TERRACLIMATE	Google Earth Engine	4638 m, monthly	2000-2023 (accessed on 12 December 2024)
Image date	Landsat L2	Google Earth Engine	30 m, 16 days	2000-2023 (accessed on 12 December 2024)
	MODIS 09A1	Google Earth Engine	500 m, 14 days	2000-2023 (accessed on 12 December 2024)
Land cover	CLCD dataset	GEE	1 m, yearly	2000-2023 (accessed on 12 December 2024)
DEM	SRTM Digital Elevation Model	NASA/GEE	30 m, NA	N/A (accessed on 12 December 2024)
Human activity	Human Footprint dataset	doi.org/10.6084/m9.figshare.16571064	1000 m, yearly	2000-2023 (accessed on 12 December 2024)

Improved CASA light use efficiency model

In this study, the Net Primary Productivity (NPP) was estimated using the improved CASA model developed by Zhu et al. (2006, 2007). Compared to the traditional CASA model (Potter et al., 1993), this improved version optimizes the calculation of absorbed photosynthetically active radiation (APAR) and environmental stress coefficients to better simulate vegetation productivity in China. The fundamental formula is expressed as *Equation 2*:

$$NPP(x,t) = (APAR)(x,t) \times \varepsilon(x,t) \quad \text{(Eq.2)}$$

where NPP(x,t) is the Net Primary Productivity of pixel x in month t; $(APAR)(x,t)$ is the photosynthetically active radiation absorbed by pixel x in month t; and ε(x,t) is the actual light use efficiency of pixel x in month t. The accuracy of the CASA model largely depends on the maximum light use efficiency (ε) parameter. This study adopted the widely recognised values proposed by Zhu et al. (2007) for different vegetation types in China. The ε values for cropland, grassland, forest, and shrubland were set to 0.542, 0.542, 0.700, and 0.429 gC/MJ, respectively.

CV value

The Coefficient of Variation (CV) serves as a classic indicator of the relative temporal stability of geospatial data (Tucker et al., 1991). Here, we utilized the CV to evaluate NPP stability in Xigaze over the last 21 years using *Equation 3*:

http://www.aloki.hu ● ISSN 1589 1623 (Print) ● ISSN 1785 0037 (Online)
DOI: http://dx.doi.org/10.15666/aeer/2402_33753391

$$Cv = \frac{1}{NPP}\sqrt{\frac{\sum_{i=1}^{n}(NPPi-\overline{NPP})}{n-1}} \quad \text{(Eq.3)}$$

where CV is the coefficient of variation, NPP_i is the NPP value for year i, n corresponds to the time series length, and $N\bar{P}P$is the mean NPP of Xigaze for the period 2000–2023. A larger CV signifies higher volatility in the NPP time series, whereas a smaller value indicates greater stability.

Trend analysis

The Theil-Sen slope estimation method determines the magnitude of a trend by calculating the median of the slopes of all data point pairs, which effectively mitigates the impact of outliers (Theil, 1950; Sen, 1968). The slope is calculated using *Equation 4*:

$$\beta = \text{Median}\left(\frac{NPP_j - NPP_k}{j-k}\right), \forall k < j \quad \text{(Eq.4)}$$

where β is the Theil-Sen slope, representing the median annual change rate of the NPP time series. The Mann-Kendall (MK) test is a non-parametric method used to examine monotonic trends in time series data (Mann, 1945; Kendall, 1975). Its statistic S is calculated as *Equation 5*:

$$S = \sum_{k=1}^{n-1}\sum_{j=k+1}^{n}\text{sgn}\left(NPP_j - NPP_k\right) \quad \text{(Eq.5)}$$

where NPP_j *and* NPP_k are the NPP values for years j and k, respectively. This study combines the Mann-Kendall test with Theil-Sen slope estimation to analyse the significance of NPP change trends in the Shigatse region.

Driver analysis based on random forest (RF) and Shapley additive explanations (SHAP)

This study employed the RF algorithm (Breiman, 2001) to model the spatial distribution of NPP. Using the dataset from the year 2020, an NPP prediction model was established based on the selected driving factors. To interpret the model, the SHAP method was applied to quantify the contribution of each feature (Lundberg and Lee, 2017). The model's performance was robust, with a coefficient of determination (R^2) of 0.90, a root mean square error (RMSE) of 15.93, a mean absolute error (MAE) of 9.09, and a sum of residuals (RES) of -0.89 (*Fig. 2*).

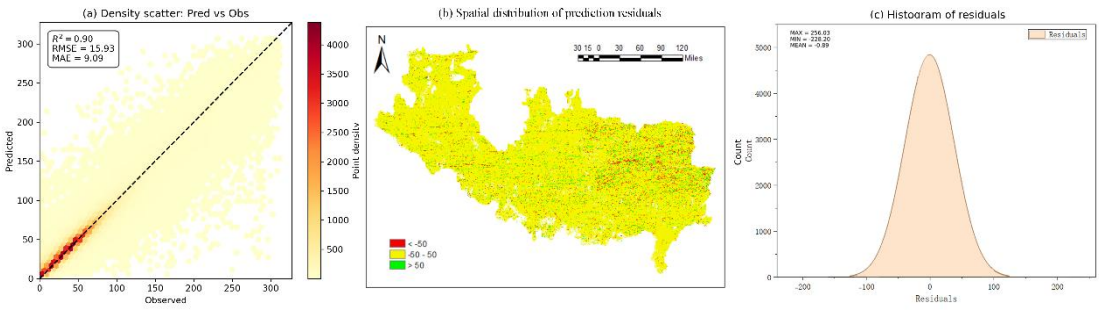

Figure 2. *Accuracy evaluation of the random forest model in predicting NPP*

http://www.aloki.hu ● ISSN 1589 1623 (Print) ● ISSN 1785 0037 (Online)
DOI: http://dx.doi.org/10.15666/aeer/2402_33753391

Results

Model performance and validation

To validate the reliability of our methodology, we first rigorously assessed the performance of the ESTARFM model. By selecting a nearly cloud-free Landsat 8 OLI image from 16 September 2020 as the ground truth, we compared it with the NDVI image reconstructed by the model for the same date. The results, as shown in the scatter plot, indicate a strong agreement between the reconstructed and actual NDVI values. The coefficient of determination (R^2) was 0.88, with a root mean square error (RMSE) of 0.049 and a mean absolute error (MAE) of 0.018. Visual comparison further confirmed that the reconstructed image accurately captured the spatial texture and details of the actual surface, demonstrating high fidelity. Subsequently, the NPP map simulated by our CASA model was compared with the national NPP product published by Zhu et al. (2007). Although a moderate correlation was found between the two datasets (Pearson's $r = 0.582$, $p < 0.001$), this is primarily attributed to the significant spatial scale mismatch between our high-resolution simulation (30 m) and the coarser national product (1 km). Therefore, the high accuracy of the NDVI reconstruction ($R2 = 0.88$) confirms the efficiency of the data fusion process, while the NPP comparison suggests that our model maintains consistency with authoritative products at the regional trend level while offering enhanced spatial detail (*Fig. 3*).

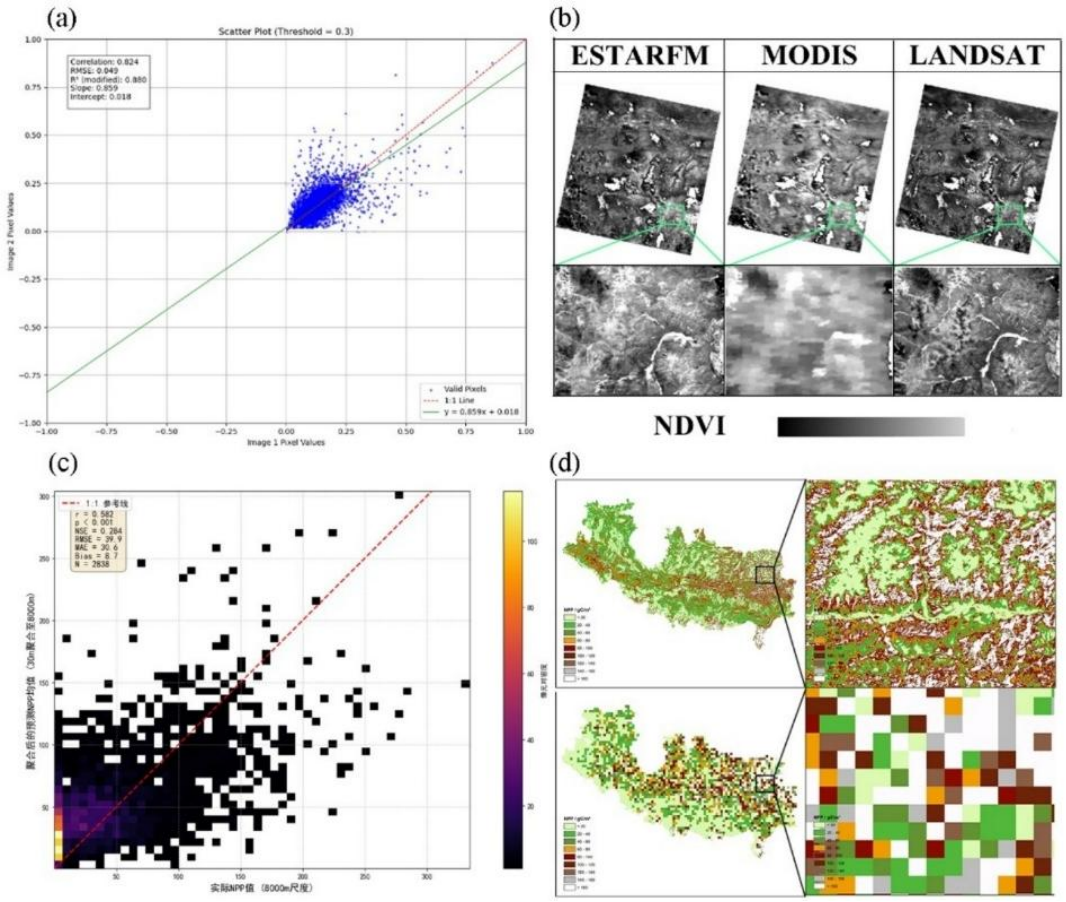

Figure 3. *Validation of the ESTARFM-CASA model. (a) Correlation between reconstructed NDVI and actual Landsat NDVI. (b) Comparison of simulated NPP with an established NPP product*

http://www.aloki.hu ● ISSN 1589 1623 (Print) ● ISSN 1785 0037 (Online)
DOI: http://dx.doi.org/10.15666/aeer/2402_33753391

Spatiotemporal dynamics of NPP (2000–2023)

During the growing season (July–September) from 2000 to 2023, the mean NPP in the Shigatse region exhibited a significant fluctuating upward trend (*Fig. 4*). The Theil-Sen slope analysis revealed an average growth rate of 0.75 g C m^{-2} $year^{-1}$ ($p < 0.01$). Over this period, NPP experienced several distinct phases of fluctuation. The lowest value occurred in 2007 (50.88 g C m^{-2}), potentially linked to lower solar radiation in that year, which inhibited photosynthetic efficiency. Conversely, the highest value was recorded in 2015 (75.32 g C m^{-2}), which may be attributed to a combination of increased grassland area and favorable precipitation conditions. After 2015, although NPP slightly decreased, it has remained at a relatively high level, benefiting from an overall increase in NDVI.

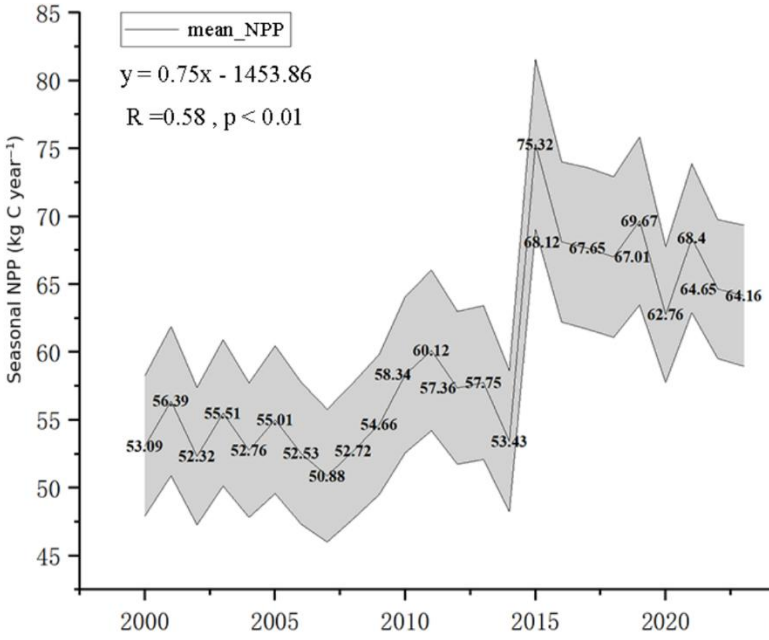

Figure 4. *Interannual variation of mean NPP in the Shigatse region from 2000 to 2023*

Spatially, the NPP in the Shigatse region demonstrated a distinct pattern of being high in the east and low in the west (*Fig. 5a, b*). Areas with higher NPP values were primarily concentrated in the eastern counties, such as Renbu and Namling, and in the southern county of Yadong. In contrast, lower NPP values were mainly distributed in the western counties of Zhongba and Saga. A comparison between the years 2023 and 2000 shows that approximately 25.72% of the region experienced a decrease in NPP, while about 5% showed no significant change. The overall spatial pattern of NPP change was characterized by an increase in the north and a decrease in the south. The coefficient of variation (CV) for NPP ranged from 0 to 3.3, with a mean of 0.474, indicating moderate overall variability. High-variability areas appeared in distinct bands along the northern and southern slopes of the Himalayas and the Gangdise mountains, as well as in the Yarlung Zangbo-Nyangchu river valley (*Fig. 5c*).

The combined Theil-Sen and Mann-Kendall trend analysis identified eight categories of NPP trends across the study area (*Fig. 6*). Over the past 23 years, approximately 40% of the region experienced an increase in NPP, with nearly 30% showing a highly significant increasing trend. This indicates a widespread and statistically significant

http://www.aloki.hu ● ISSN 1589 1623 (Print) ● ISSN 1785 0037 (Online)
DOI: http://dx.doi.org/10.15666/aeer/2402_33753391

improvement in vegetation productivity in most parts of the region. The most significant increases were observed in the middle reaches of the Yarlung Zangbo River, including parts of Lhatse, Renbu, and Xaitongmoin counties, where the average annual NPP growth rate exceeded 2.47 g C m^{-2}. Conversely, about 18% of the area experienced a decrease in NPP, with over 12% showing a highly significant decrease, suggesting that risks of ecological degradation persist. These decreasing trends were sporadically distributed in high-altitude areas and in Yadong County on the southern slope of the Himalayas. Approximately 34% of the region showed no statistically significant trend, where NPP remained relatively stable.

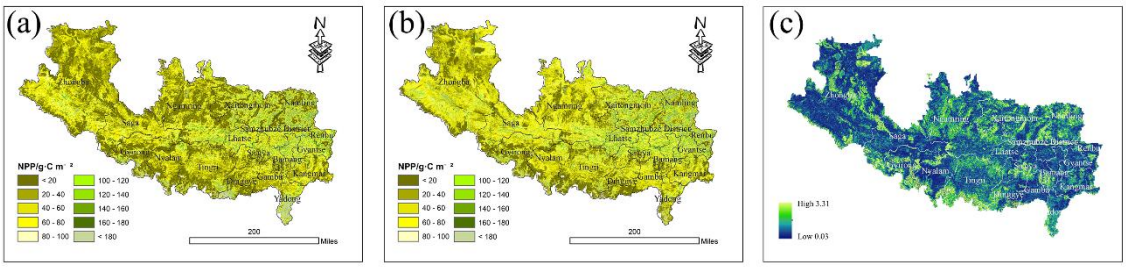

Figure 5. *Spatial patterns of NPP in Shigatse. (b) Mean NPP in 2023. (c) Coefficient of variation (CV) of NPP from 2000 to 2023*

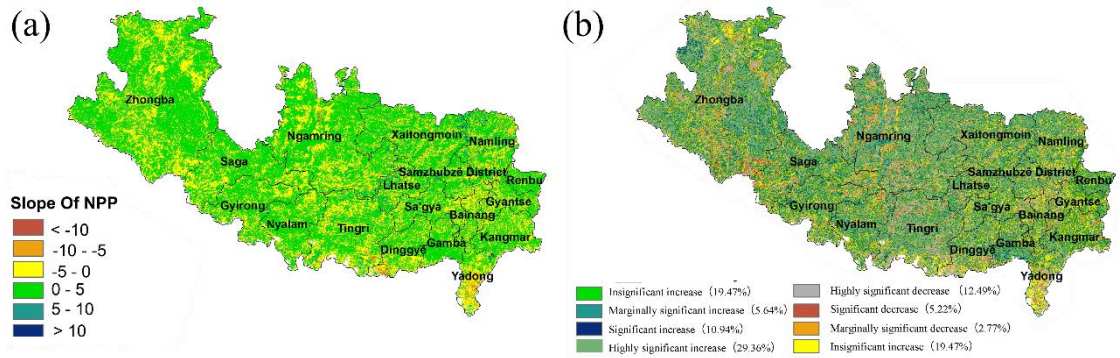

Figure 6. *NPP trend analysis from 2000 to 2023. (a) Spatial distribution of the Theil-Sen slope. (b) Spatial distribution of the Mann-Kendall significance test results*

Impact of land use/cover change (LUCC) on NPP

Analysis of land use/cover change between 2000 and 2023 reveals the underlying drivers of NPP dynamics in the Shigatse region. As shown in *Table 2,* grassland was the dominant land cover type, accounting for over 88% of the total area, and its coverage showed an increasing trend over the study period. Barren land was the largest source of land cover conversion, with a total of 11,174.33 km^2 transitioning to other types, resulting in a net decrease of 8598.43 km^2. The primary conversion pathway was from barren land to grassland, which accounted for 10,315.94 km^2, representing 92.31% of the total loss from barren land. Grassland experienced the largest net gain in area, increasing from 147,213.2 km^2 in 2000 to 155,660.3 km^2 in 2023, a net increase of 8447.16 km^2 (5.74%). This expansion was overwhelmingly contributed by the conversion of barren land, which accounted for 96.81% of the newly added grassland.

http://www.aloki.hu ● ISSN 1589 1623 (Print) ● ISSN 1785 0037 (Online)
DOI: http://dx.doi.org/10.15666/aeer/2402_33753391

Table 2. *Land use/cover area and its changes in Shigatse from 2000 to 2023*

LUCC	Area in 2000 (km²)	Area in 2023 (km²)	Net change (km²)	Change rate (%)
Cropland	21.53	11.11	-10.43	-48.42
Forest	1208.03	1322.44	114.41	9.47
Shrub	1.93	10.14	8.20	424.79
Grassland	147213.20	155660.30	8447.16	5.74
Water	3327.99	3355.93	27.94	0.84
Snow/Ice	3823.37	3832.29	8.92	0.23
Barren	20617.24	12018.81	-8598.43	-41.71
Impervious	0.01	0.68	0.68	67000.00
Wetland	3.27	4.83	1.56	47.76

In terms of NPP gains and losses driven by LUCC, the total NPP in 2023 was higher than in 2000, with LUCC contributing a net increase of approximately 112.03 GgC. As illustrated in *Figure 7,* the expansion of grassland, primarily driven by climate change, was the main engine of the NPP increase, accounting for 84.82% of the net gain. Specifically, the conversion of barren land to grassland resulted in an annual NPP increase of about 95.76 GgC. Additionally, the melting of some snow and ice, which transitioned into barren land and grassland, contributed gains of 4.59 GgC and 7.61 GgC, respectively. The conversion of grassland to forest also led to an NPP increase of 9.15 GgC. Meanwhile, certain land use changes also caused NPP losses. For example, the degradation of some grassland into barren land resulted in an NPP loss of 7.01 GgC. Overall, the NPP changes resulting from transitions between non-barren and grassland types were relatively balanced (*Fig. 8*).

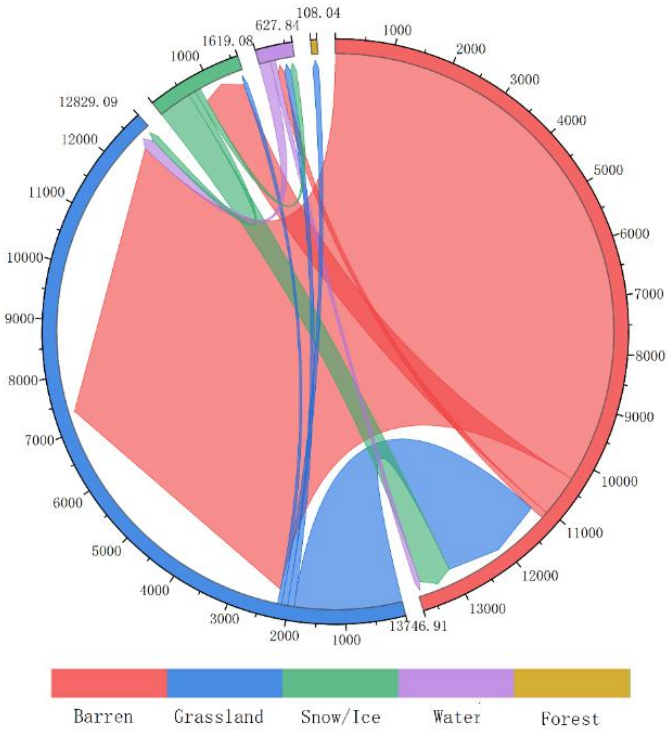

Figure 7. *Land use/cover transfer matrix from 2000 to 2023*

http://www.aloki.hu ● ISSN 1589 1623 (Print) ● ISSN 1785 0037 (Online)
DOI: http://dx.doi.org/10.15666/aeer/2402_33753391

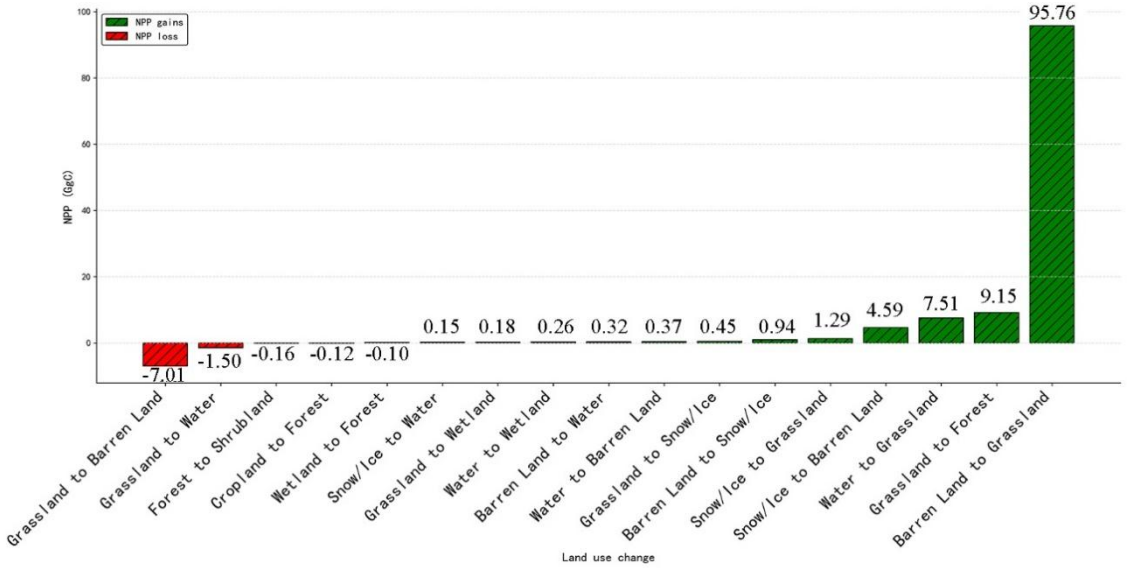

Figure 8. *Changes in NPP caused by major land use/cover transitions*

Furthermore, an analysis of the mean NPP for each land cover type shows a general increase across all categories between 2000 and 2023 (*Fig. 9*). The unit-area NPP for various types, including grassland, barren land, shrubland, forest, and cropland, all increased. This indicates a significant improvement in the ecological environment of the Shigatse region over the past two decades. The more favorable ecological conditions provided better growing conditions for plants across different land use types, thereby boosting the overall NPP.

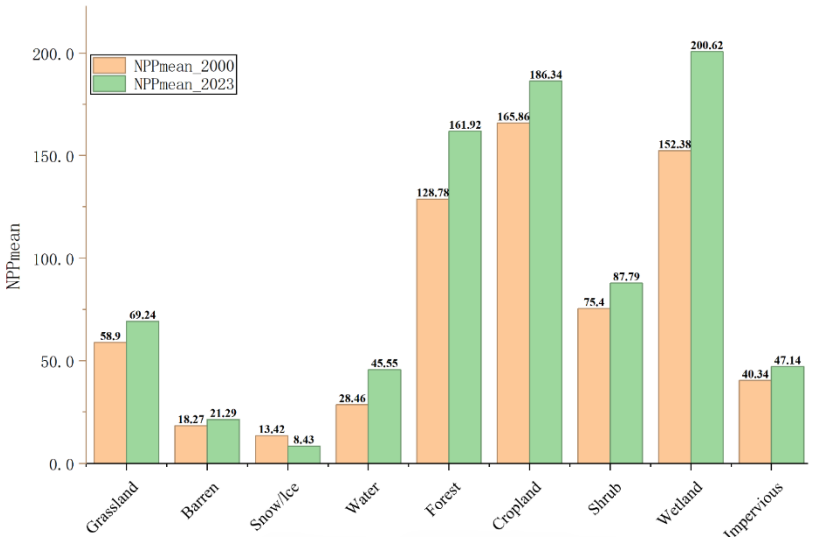

Figure 9. *Mean NPP for different land use/cover types in 2000 and 2023*

Analysis of driving factors based on RF-SHAP

Importance of driving factors

To further quantify the contribution of each driving factor to NPP, a SHAP analysis was performed on the NPP and driver datasets (*Fig. 10*). The importance of each factor,

http://www.aloki.hu ● ISSN 1589 1623 (Print) ● ISSN 1785 0037 (Online)
DOI: http://dx.doi.org/10.15666/aeer/2402_33753391

ranked by its mean absolute SHAP value, is shown in *Figure 10a*. The order was as follows: Elevation (DEM) > Precipitation (PRE) > Solar radiation (SOLAR) > Human footprint (HF) > Temperature (TEMP). DEM was the most significant contributor with a mean SHAP value of 12.51, followed closely by PRE at 11.84. In contrast, TEMP had the smallest contribution, with a value of only 2.84.

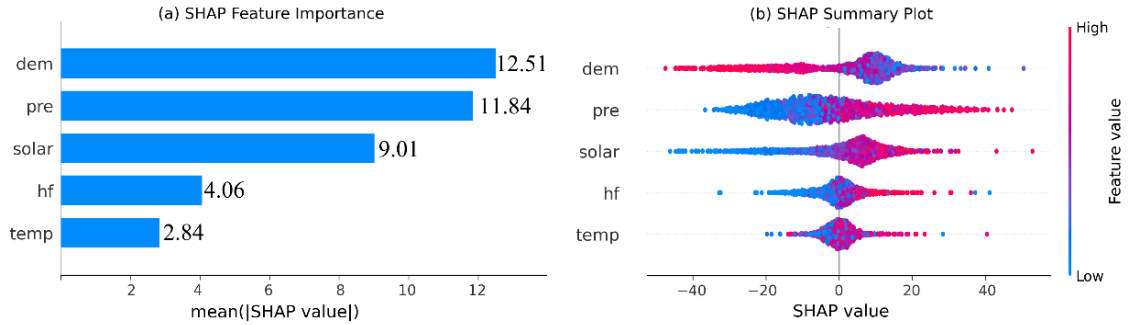

Figure 10. *Results of the SHAP analysis for NPP drivers. (a) Mean absolute SHAP values indicating feature importance. (b) SHAP summary plot showing the impact of each feature on model output*

The SHAP summary plot (*Fig. 10b*) reveals the nature of the relationship between each driver and NPP. Elevation (DEM) exhibited a clear negative correlation with NPP. Low elevation values (indicated by blue dots) are predominantly on the positive side of the SHAP value axis, suggesting that lower altitudes promote NPP accumulation. Conversely, high elevation values (red dots) are concentrated on the negative SHAP value side, indicating a strong inhibitory effect on NPP growth as altitude increases. Precipitation (PRE) showed a generally positive relationship with NPP. Higher precipitation values are clustered on the positive SHAP side, contributing positively to NPP, while lower precipitation acts as a limiting factor. Solar radiation also demonstrated a positive driving effect, with high radiation values associated with positive SHAP values, thus enhancing NPP. Low solar radiation, especially when strongly negative SHAP values are present, highlights the significant adverse impact of poor light conditions on NPP. The effects of human footprint (HF) and temperature (TEMP) were more complex, with both high and low values appearing on both sides of the SHAP axis, suggesting their impact on NPP may be context-dependent or interactive with other variables.

Interaction effects of driving factors

To explore the interaction effects among the driving factors, we further analysed the interplay between the top five drivers: DEM, Precipitation (PRE), temperature (TEMP), Solar radiation (SOLAR), and human footprint (HF). The analysis revealed significant non-linear relationships and interaction effects (*Fig. 11*).

The effect of elevation on NPP showed a distinct inverted “U” shaped non-linear pattern (*Fig. 11a1*). SHAP values were negative at elevations below approximately 4500 m and above 5800 m, indicating that both excessively low and high altitudes are unfavorable for NPP accumulation. The peak positive effect occurred in the 5000–5500 m range. This is likely because the 3000–4500 m zone in the study area, despite suitable soil and thermal conditions for alpine meadows and shrubs, may be subject to human activity

http://www.aloki.hu ● ISSN 1589 1623 (Print) ● ISSN 1785 0037 (Online)
DOI: http://dx.doi.org/10.15666/aeer/2402_33753391

or drought stress. Areas above 5000 m face limitations from low temperatures and exposed bedrock. Interaction plots show that sufficient precipitation amplifies the positive effect of optimal elevation on NPP, while human activity, even in climatically suitable areas, tends to suppress NPP potential.

Precipitation's impact on NPP displayed a threshold effect around 100 mm (*Fig. 11b1*). When precipitation increased from low levels (<50 mm) to moderate levels (100 mm), the SHAP value rapidly shifted from negative to positive, indicating that low precipitation is a major limiting factor for NPP. However, once precipitation exceeded this threshold, its positive effect plateaued and even slightly declined, which could be associated with increased cloud cover and reduced solar radiation during periods of high rainfall.

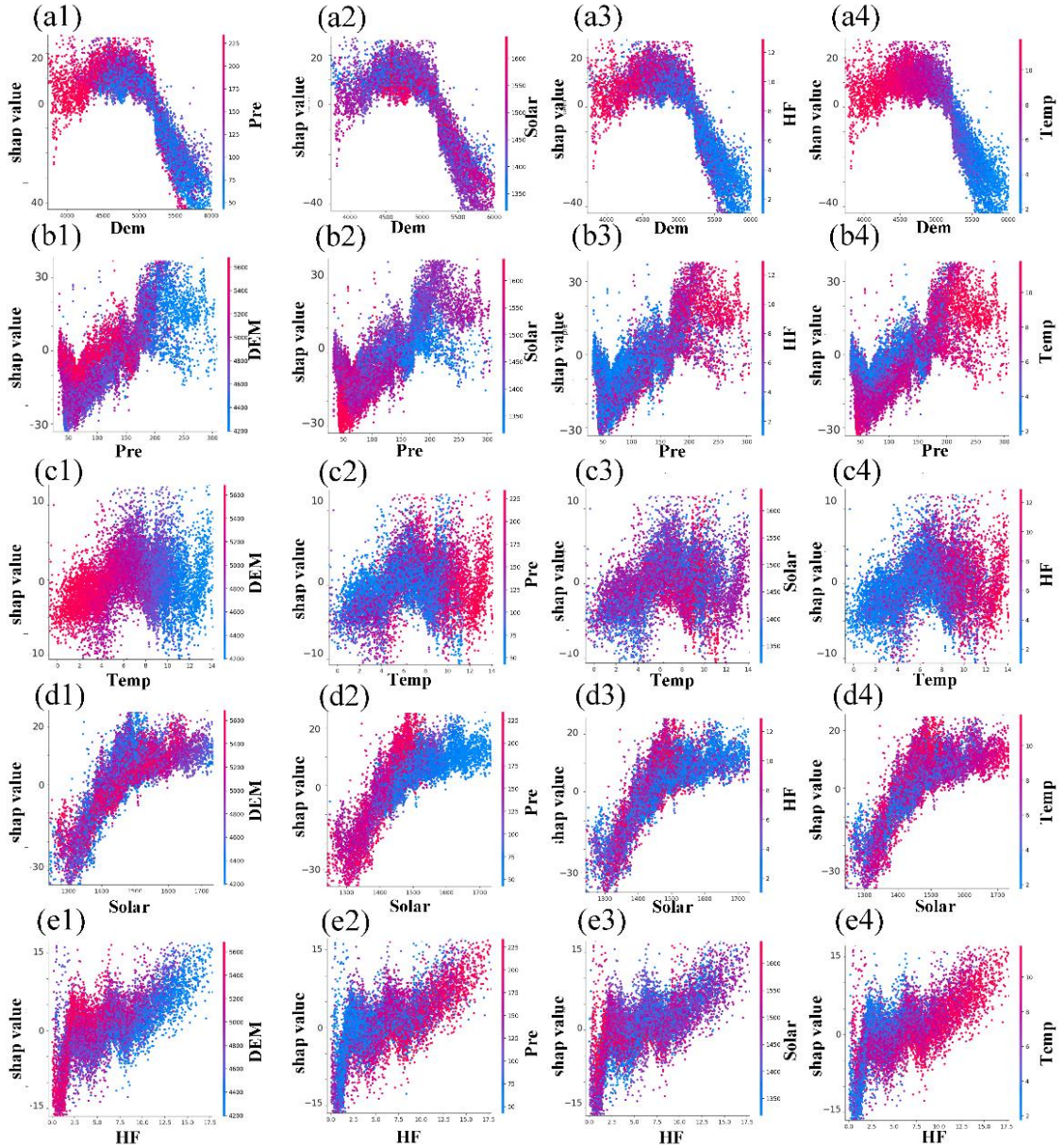

Figure 11. *SHAP interaction plots for the main driving factors of NPP. Abbreviations: DEM, Digital Elevation Model; PRE, Precipitation; TEMP, Temperature; SOLAR, Solar Radiation; HF, Human Footprint*

http://www.aloki.hu ● ISSN 1589 1623 (Print) ● ISSN 1785 0037 (Online)
DOI: http://dx.doi.org/10.15666/aeer/2402_33753391

Solar radiation and temperature demonstrated a synergistic positive effect on NPP (*Fig. 11c1, d1*). As a fundamental energy source for photosynthesis, solar radiation had a clear and strong positive impact. Specifically, the SHAP dependence analysis identified a critical threshold at approximately 1400 MJ/m², above which the positive contribution to NPP increased sharply. This trend is reflected by the steep upward slope in the interaction plot. The influence of temperature was more complex but generally positive. The interaction between human footprint (HF) and elevation revealed a strong spatial dependency. Almost all strongly positive SHAP values for HF were concentrated in the 4200–4800 m elevation range, possibly linked to significant afforestation and grassland restoration projects in the Shigatse region.

Discussion

Analysis of NPP trends and land use change impacts

This study reveals a significant increasing trend in Net Primary Productivity (NPP) in the climate-sensitive Shigatse region over the past two decades. This finding aligns with the "Global Greening" phenomenon observed in the satellite era, where China has been identified as a leading contributor (Chen et al., 2019; Zhu et al., 2016). While local heterogeneity exists, the "high-east, low-west" spatial pattern identified in our research is consistent with the broad bioclimatic gradient of the Tibetan Plateau described in previous large-scale assessments (Piao et al., 2020).

Our analysis further pinpoints that the primary driver of this NPP increase was the large-scale conversion of barren land to grassland, a process that contributed over 84% of the net NPP gain. This suggests that vegetation recovery in this region is driven not only by physiological enhancement due to warming but also by structural expansion of vegetation cover. This mirrors the findings of Bryan et al. (2018), who highlighted that China's major ecological restoration programs also have successfully reversed desertification and enhanced carbon sinks. From a temporal perspective, the sustained high levels of NPP following the 2015 peak correspond with the intensification of regional environmental policies. Statistics indicate that from 2016 to 2020, artificially planted grassland in Shigatse expanded by approximately 23,667 ha (Ren et al., 2022). This confirms that anthropogenic interventions, when scientifically managed, can effectively synergize with climate warming to boost ecosystem productivity in high-altitude semi-arid regions.

Driving mechanisms of NPP variation

Ecological processes are rarely linear. By employing the SHAP-based approach, we quantified the non-linear contributions of environmental drivers. Elevation emerged as the dominant factor (SHAP value: 12.51), exhibiting a distinct threshold effect where the positive contribution rapidly diminishes above 5000 m. This "inverted U-shape" pattern is consistent with the global alpine treeline and vegetation limit theory, which posits that low temperatures and physiological drought at extreme altitudes impose an insurmountable metabolic cap on photosynthesis (Körner, 2007; Paulsen and Körner, 2014).

Our study further revealed that NPP in Shigatse is highly sensitive to precipitation, with a critical threshold identified at approximately 100 mm. Below this level, water availability acts as a strict inhibitor, aligning with the "Pulse-Reserve" paradigm in arid

http://www.aloki.hu ● ISSN 1589 1623 (Print) ● ISSN 1785 0037 (Online)
DOI: http://dx.doi.org/10.15666/aeer/2402_33753391

ecosystem ecology (Huxman et al., 2004). Notably, the SHAP interaction analysis uncovered an antagonistic effect between precipitation and solar radiation. Increased rainfall often coincides with increased cloud cover, thereby reducing photosynthetically active radiation (PAR). This trade-off mechanism explains why NPP does not increase linearly with precipitation, a phenomenon widely observed in monsoon-dominated regions (Nemani et al., 2003). Unlike linear regression models, our RF-SHAP framework successfully captured this radiation-limited regime during the peak growing season.

Regarding anthropogenic factors, the impact appeared spatially heterogeneous. While urbanization exerts local negative pressures, the broad-scale positive effects of ecological restoration (e.g., enclosure of grazing lands) are evident. This duality highlights the complexity of "human-nature" coupled systems in the Anthropocene, where humans act as both a disturbance and a restoration agent (Ellis et al., 2013).

Limitations and future perspectives

Despite the systematic analysis, this study has limitations. First, the reliance on optical remote sensing (Landsat/MODIS) is inherently constrained by cloud cover, a persistent challenge in the Himalayas during the monsoon season. This necessitated narrowing our research window to the late growing season (July–September). Future research could integrate microwave remote sensing (e.g., Vegetation Optical Depth, VOD) or Solar-Induced Fluorescence (SIF) to monitor vegetation dynamics independent of weather conditions (Reichstein et al., 2019). Second, while we identified elevation and precipitation as dominant drivers, the current model simplifies soil properties. Incorporating high-resolution soil moisture and nutrient data could further refine the mechanistic understanding of NPP heterogeneity (Crowther et al., 2016). Finally, combining data-driven machine learning models with process-based physiological models represents a promising direction to validate statistical relationships with biological mechanisms under future climate scenarios (Reichstein et al., 2019).

Conclusion

This study integrated multi-source remote sensing data, coupled with the ESTARFM, CASA, and explainable machine learning models, to systematically investigate the spatiotemporal dynamics and complex driving mechanisms of Net Primary Productivity (NP) in the climate-sensitive Shigatse region from 2000 to 2023. The main conclusions are as follows:

(1) The NPP in the Shigatse region exhibited a significant increasing trend, with the conversion of land cover types—specifically from barren land to grassland—being the direct and primary cause. This transition was the main driver of the net NPP increase.

(2) Elevation is the dominant factor controlling the spatial heterogeneity of NPP. Above 5000 m, harsh low-temperature conditions and poor soil constitute strong limitations on vegetation growth. In some lower-altitude areas, NPP accumulation is also constrained by human activities or drought stress.

(3) Climatic factors exhibit threshold effects and complex interactions. A cumulative precipitation of around 100 mm was identified as a key threshold. Solar radiation consistently showed a positive driving effect. The impacts of temperature and human footprint are highly dependent on their interaction with other dominant factors, such as elevation and precipitation.

http://www.aloki.hu ● ISSN 1589 1623 (Print) ● ISSN 1785 0037 (Online)
DOI: http://dx.doi.org/10.15666/aeer/2402_33753391

In summary, the ecological condition of the Shigatse region has significantly improved over the past two decades, benefiting from both the optimization of land use structure and favorable regional hydrothermal and climatic conditions. This research highlights the non-linear responses and complex coupled effects of driving factors, underscoring the critical importance of considering multi-scale, multi-element synergistic effects when assessing and managing high-altitude ecosystems.

Acknowledgements. This study was supported by the Postgraduate Education Innovation Program of Xizang Agricultural and Animal Husbandry University (Project No.: YJS2025-29), and the Xizang Agriculture and Animal Husbandry University Doctoral Program in Forestry (Phase I) (Grant No. 533325001).

REFERENCES

[1] Basang, C., Wen, Z., Liu, Y., et al. (2022): Analysis of the spatial-temporal evolution patterns of grassland net primary productivity and its driving mechanisms in Tibet. – Acta Agrestia Sinica 30(4): 778-789. DOI: 10.11733/j.issn.1007-0435.2022.04.002 (in Chinese).

[2] Bryan, B. A., Gao, L., Ye, Y., et al. (2018): China's response to a national land-system sustainability emergency. – Nature 559(7713): 193-204. DOI: 10.1038/s41586-018-0280-2.

[3] Cai, M., Yang, S., Zhao, C., et al. (2017): Insight into runoff characteristics using hydrological modeling in the data-scarce southern Tibetan Plateau: past, present, and future. – PLoS ONE 12(5): e0176813. DOI: 10.1371/journal.pone.0176813.

[4] Chen, C., Park, T., Wang, X., et al. (2019): China and India lead in greening of the world through land use management. – Nature Sustainability 2(2): 122-129. DOI: 10.1038/s41893-019-0220-7.

[5] Crowther, T. W., Todd-Brown, K. E. O., Rowe, C. W., et al. (2016): Quantifying global soil carbon losses in response to warming. – Nature 540(7631): 104-108. DOI: 10.1038/nature20150.

[6] Dunzhu, C., Shi, Y. (2000): An Analysis of Climatic Variability in Rikaze from 1956 to 1997. – Meteorological Monthly 26(1): 26-31. DOI: 10.7519/j.issn.1000-0526.2000.1.010 (in Chinese).

[7] Ellis, E. C., Kaplan, J. O., Fuller, D. Q., et al. (2013): Used planet: a global history. – Proceedings of the National Academy of Sciences 110(20): 7978-7985. DOI: 10.1073/pnas.1217241110.

[8] Emelyanova, I. V., McVicar, T. R., Van Niel, T. G., et al. (2013): Assessing the accuracy of blending Landsat–MODIS surface reflectances in two landscapes with contrasting spatial and temporal dynamics: a framework for algorithm selection. – Remote Sensing of Environment 133: 193-209. DOI: 10.1016/j.rse.2013.02.007.

[9] Field, C. B., Behrenfeld, M. J., Randerson, J. T., et al. (1998): Primary production of the biosphere: integrating terrestrial and oceanic components. – Science 281(5374): 237-240. DOI: 10.1126/science.281.5374.237.

[10] Forster, P. M., Smith, C., Walsh, T., et al. (2024): Indicators of Global Climate Change 2023: annual update of key indicators of the state of the climate system and human influence. – Earth System Science Data 16(6): 2625-2658. DOI: 10.5194/essd-15-2295-2023.

[11] Gao, Z., Ding, W., He, J. (2020): Land cover classification and dynamic monitoring in Shigatse based on random forest algorithm and MODIS data. – Journal of Anhui Agricultural Sciences 48(16): 1-12. DOI: 10.3969/j.issn.0517-6611.2020.16.001 (in Chinese).

http://www.aloki.hu ● ISSN 1589 1623 (Print) ● ISSN 1785 0037 (Online)
DOI: http://dx.doi.org/10.15666/aeer/2402_33753391

[12] Huxman, T. E., Smith, M. D., Fay, P. A., et al. (2004): Convergence across biomes to a common rain-use efficiency. – Nature 429(6992): 651-654. DOI: 10.1038/nature02561.
[13] Jiang, Y. (2017): Ecological Environmental Quality Assessment of Shigatse on 3S. – Sichuan Normal University, Chengdu. DOI: CNKI:CDMD:2.1017.160249 (in Chinese).
[14] Kendall, M. G. (1975): Rank Correlation Methods. 4th Ed. – Charles Griffin, London.
[15] Körner, C. (2007): The use of 'altitude' in ecological research. – Trends in Ecology & Evolution 22(11): 569-574. DOI: 10.1016/j.tree.2007.09.006.
[16] Li, H., Tan, Z., Gui, X., et al. (2025): The resistance and recovery responses of vegetation to compound drought-heat events in China and their driving factors analysis over the past 40 years. – Acta Ecologica Sinica 45(24): 12288-12305. DOI: 10.20103/j.stxb.202503160590 (in Chinese).
[17] Lundberg, S. M., Lee, S. I. (2017): A unified approach to interpreting model predictions – Advances in Neural Information Processing Systems 30: 4765-4774. DOI: 10.48550/arXiv.1705.07874.
[18] Mann, H. B. (1945): Nonparametric tests against trend. – Econometrica 13: 245-259. DOI: 10.2307/1907187.
[19] Mayer, A., Kaufmann, L., Kalt, G., et al. (2021): Applying the human appropriation of net primary production framework to map provisioning ecosystem services and their relation to ecosystem functioning across the European Union. – Ecosystem Services 51: 101344. DOI: 10.1016/j.ecoser.2021.101344.
[20] Naeem, S., Zhang, Y., Tian, J., et al. (2020): Quantifying the impacts of anthropogenic activities and climate variations on vegetation productivity changes in China from 1985 to 2015. – Remote Sensing 12(7): 1113. DOI: 10.3390/rs12071113.
[21] Nayak, A., Matta, G., Uniyal, D. P. (2023): Hydrochemical characterization of groundwater quality using chemometric analysis and water quality indices in the foothills of Himalayas. – Environment, Development and Sustainability 25(12): 14229-14260. DOI: 10.1007/s10668-022-02661-4.
[22] Nemani, R. R., Keeling, C. D., Hashimoto, H., et al. (2003): Climate-driven increases in global terrestrial net primary production from 1982 to 1999. – Science 300(5625): 1560-1563. DOI: 10.1126/science.1082750.
[23] Paulsen, J., Körner, C. (2014): A climate-based model to predict potential treeline position around the globe. – Alpine Botany 124(1): 1-12. DOI: 10.1007/s00035-014-0124-0.
[24] Peng, Z., Liu, W., Tian, R. (2021): Effects of altitude and aspect on soil extracellular enzyme activities in Tanggula Mountain. – Acta Ecologica Sinica 41(19): 7659-7668. DOI: 10.5846/stxb201909231984 (in Chinese).
[25] Piao, S., Wang, X., Park, T., et al. (2020): Characteristics, drivers and feedbacks of global greening. – Nature Reviews Earth & Environment 1(1): 14-27. DOI: 10.1038/s43017-019-0001-x.
[26] Potter, C. S., Randerson, J. T., Field, C. B., et al. (1993): Terrestrial ecosystem production: a process model based on global satellite and surface data. – Global Biogeochemical Cycles 7(4): 811-841. DOI: 10.1029/93GB02725.
[27] Reichstein, M., Camps-Valls, G., Stevens, B., et al. (2019): Deep learning and process understanding for data-driven Earth system science. – Nature 566(7743): 195-204. DOI: 10.1038/s41586-019-0912-1.
[28] Ren, L., Xia, C., Yu, F. (2022): Practical exploration of ecological civilization construction in a typical plateau border city: a case study of Shigatse. – Modern Horticulture 45(23): 181-185. DOI: 10.3969/j.issn.1006-4958.2022.23.067 (in Chinese).
[29] Running, S. W., Nemani, R. R., Heinsch, F. A., et al. (2004): A continuous satellite-derived measure of global terrestrial primary production. – BioScience 54(6): 547-560. DOI: 10.1641/0006-3568(2004)054[0547:ACSMOG]2.0.CO;2.
[30] Scholze, M., Knorr, W., Arnell, N. W., et al. (2006): A climate-change risk analysis for world ecosystems. – Proceedings of the National Academy of Sciences 103(35): 13116-13120. DOI: 10.1073/pnas.0601816103.

http://www.aloki.hu ● ISSN 1589 1623 (Print) ● ISSN 1785 0037 (Online)
DOI: http://dx.doi.org/10.15666/aeer/2402_33753391

[31] Sen, P. K. (1968): Estimates of the regression coefficient based on Kendall's tau. – Journal of the American Statistical Association 63(324): 1379-1389. DOI: 10.1080/01621459.1968.10480934.
[32] Theil, H. (1950): A rank-invariant method of linear and polynomial regression analysis. I, II, III. – Indagationes Mathematicae 12: 386-392.DOI: 10.1007/978-94-011-2546-8_20.
[33] Tucker, C. J., Newcomb, W. W., Los, S. O., et al. (1991): Mean and inter-year variability of growing-season normalized difference vegetation index for the Sahel 1981–1989. – International Journal of Remote Sensing 12(6): 1133-1135. DOI: 10.1080/01431169108929717.
[34] Wang, Q., Zhang, Y., Onojeghuo, A. O., et al. (2017): Enhancing spatio-temporal fusion of MODIS and Landsat data by incorporating 250 m MODIS data. – IEEE Journal of Selected Topics in Applied Earth Observations and Remote Sensing 10(9): 4116-4123. DOI: 10.1109/JSTARS.2017.2701643.
[35] Wang, R., Sun, Y., Zong, J., et al. (2024): Remote sensing application in ecological restoration monitoring: a systematic review. – Remote Sensing 16(12): 2204. DOI: 10.3390/rs16122204.
[36] Wu, M., Wu, C., Huang, W., et al. (2016): An improved high spatial and temporal data fusion approach for combining Landsat and MODIS data to generate daily synthetic Landsat imagery. – Information Fusion 31: 14-25. DOI: 10.1016/j.inffus.2015.12.005.
[37] Wu, K., Zhou, C., Zhang, Y., et al. (2022): Long-term spatiotemporal variation of net primary productivity and its correlation with the urbanization: a case study in Hubei Province, China. – Frontiers in Environmental Science 9: 808401. DOI: 10.3389/fenvs. 2021.808401.
[38] Xu, S., Zhang, M. (2024): Spatial-temporal evolution of net primary productivity of grasslands on the Qinghai-Xizang Plateau from 1978 to 2020. – Journal of Glaciology and Geocryology 46(3): 1028-1042. DOI: 10.7522/j.issn.1000-0240.2024.0082 (in Chinese).
[39] Zhang, J., Qi, Y., Yang, R., et al. (2023): Impacts of climate change and land use/cover change on the net primary productivity of vegetation in the Qinghai Lake Basin. – International Journal of Environmental Research and Public Health 20(3): 2179. DOI: 10.3390/ijerph20032179.
[40] Zhou, H., Shang, K., Wang, S. (2011): Analysis of climate change characteristics in Shigatse in recent 53 years. – Meteorological Science and Technology 39(02): 165-171. DOI: 10.3969/j.issn.1671-6345.2011.02.007 (in Chinese).
[41] Zhu, W., Pan, Y., He, H. (2006): Simulation of maximum light use efficiency for some typical vegetation types in China. – Chinese Science Bulletin 51(4): 457-463. DOI: 10.3321/j.issn:0023-074X.2006.06.014.
[42] Zhu, W., Pan, Y., Zhang, J. (2007): Estimation of net primary productivity of Chinese terrestrial vegetation based on remote sensing. – Journal of Plant Ecology 31(3): 413-424. DOI: 10.17521/cjpe.2007.0050.
[43] Zhu, X., Chen, J., Gao, F., et al. (2010): An enhanced spatial and temporal adaptive reflectance fusion model for complex heterogeneous regions. – Remote Sensing of Environment 114(11): 2610-2623. DOI: 10.1016/j.rse.2010.05.032.
[44] Zhu, Z., Piao, S., Myneni, R. B., et al. (2016): Greening of the Earth and its drivers. – Nature Climate Change 6(8): 791-795. DOI: 10.1038/NCLIMATE3004.
[45] Breiman, L. (2001): Random forests. – Machine Learning 45(1): 5-32. DOI: 10.1023/A:1010933404324,

http://www.aloki.hu ● ISSN 1589 1623 (Print) ● ISSN 1785 0037 (Online)
DOI: http://dx.doi.org/10.15666/aeer/2402_33753391